J. Inst. Eng. India Ser. C (April 2020) 101(2):407–413
https://doi.org/10.1007/s40032-019-00542-w

CASE STUDY

Synthesis and Characterization of Alumina Nanoparticles: A Case Study

Neeraj Kumar Bhoi[1] · **Harpreet Singh**[1] · **Saurabh Pratap**[1]

Received: 1 October 2018 / Accepted: 14 November 2019 / Published online: 22 November 2019

Abstract Alumina nanoparticles (Al_2O_3 NPs) were successfully prepared from aluminum nitrate precursor and methanol using the precipitation method, while NaOH was added after stirring. The prepared Al_2O_3 NPs were synthesized at the calcination temperature of 400 °C and 600 °C for 2 h. Later, the synthesized Al_2O_3 NPs were characterized by X-ray diffraction and scanning electron microscopy analysis. The conducted experiments show that the calcination temperature was found to have a strong influence on the Al_2O_3 NPs' stability and processing time. It was clearly observed that with the increase in calcination temperature the crystallite size of the sample increases, indicating the enhanced crystallinity. The crystallite size of the synthesized Al_2O_3 NPs was in the range of 53–72 nm. The economic analysis of the produced Al_2O_3 NPs has indicated that the precipitation method is cost-effective.

Keywords Al_2O_3 · Nanoparticles · Precipitation · XRD · SEM · Cost-effective

Introduction

Aluminum and its compounds are well known for their different properties which were used in a wide range of industrial applications. A range of aluminum and different alloys are used in mechanical, aerospace, chemical, nuclear, spacecraft, electronics, sensors and actuator devices, and medical science applications [1]. Aluminum oxide (Al_2O_3) is one of its kinds of compound which is widely used in process metallurgy to enhance the mechanical properties of the matrix material and coolant applications in microelectromechanical systems (MEMS) due its lower density and better solubility. Al_2O_3 is having different phases such as gamma, delta, theta, and alpha. There are a number of synthesis techniques that were widely developed and accepted for the preparation of Al_2O_3 nanoparticles (Al_2O_3 NPs), namely solgel synthesis [2], precipitation method [2], DC thermal plasma synthesis, hydrothermal synthesis, pyrolysis, combustion synthesis [3, 4], mechanochemical synthesis [5], etc.

A perfect crystal can extent infinitely in all the directions, but no crystal can be treated as a perfect crystal due to deviation in the pattern and impurities during the synthesis process. However, the symmetry XRD pattern and peak broadening define the level of lattice strain and crystallite size. In the case of polycrystalline material, the crystallite size can be termed as particle size due to agglomeration of the crystals. The crystallite size and lattice strain are in direct relation to peak width and intensity [6]. There is an increase in the synthesis of Al_2O_3 NPs due to their unique physical and material properties which exhibit wide application area. Khalil et al. synthesized the Al_2O_3 NPs by the flame hydrolysis, polymeric route, and solgel method. It was observed that nanoparticles prepared by the flame hydrolysis method have lower particle size than the other two processes adopted for preparation (particle size obtained as less than 20 nm, 75 nm and 50 nm in flame hydrolysis, polymeric route, and solgel techniques, respectively). With the higher calcination temperature, lower specific surface area was achieved in all the three experimental conditions with lower in case of flame hydrolysis condition [1]. Mimani synthesized the Al_2O_3 NPs with aluminum nitrate and urea with the help of

✉ Neeraj Kumar Bhoi
neerajbitd@gmail.com

[1] Indian Institute of Information Technology Design and Manufacturing, Jabalpur, Jabalpur, India

the combustion method. With the rapid heating of precursor and reducing agent at a temperature of 450 to 500 °C in Bunsen burner or hot plate left with the end of alpha alumina particles [3], two different precursors, inorganic and organic (i.e., inorganic aluminum chloride ($AlCl_3$) and organic aluminimtriisopropylate (C_3H_7O)3Al)), were used for the synthesis of Al_2O_3 NPs using the solgel method by Rogojan et al. Needle-shaped and spherical-type particles were obtained with the average particle size of below 25 and 20 nm, respectively. Higher heating temperature (i.e, above 1000 °C) leads to the formation of single-phase crystalline alpha alumina [7]. Rajaeiyan et al. compares the solgel and co-precipitation methods during the formation of nanostructured γ and α alumina powder. A higher temperature is required in the case of solgel techniques but having advantages of more uniform and sharp peak of alumina than the co-precipitation method. With solgel techniques, α alumina nanoparticles are obtained in the range of 10–20 nm size, while 10–50-nm-size particles were observed in the case of co-precipitation method of processing [2]. With the use of dodecyltrimethylammonium bromide (DTAB) as the surfactant, the synthesized alumina nanoparticle size was obtained as 27 nm [8]. Table 1 summarizes the various techniques adopted for the synthesis of the Al_2O_3 NPs and size obtained during the synthesis. As an outcome, the synthesized Al_2O_3 NPs may not seriously have been addressed. In this paper, the synthesis of Al_2O_3 NPs by the precipitation displacement reaction between aluminum nitrate precursor ($Al(NO_3)_3\_9H_2O$) and methanol (CH_3OH) and subsequent thermal treatment was reported.

Experimental Detail

Materials

Aluminum nitrate Al $(NO_3)_3\_9H_2O$ (assay > 99.997%), methanol (CH_3OH), sodium hydroxide pellets (NaOH), and deionized water were used as starting precursors for the synthesis of Al_2O_3 NPs. All the raw materials were supplied by Alpha Chemika Ltd., Mumbai, India. The chemicals were used without further purification.

Synthesis of Al_2O_3 NPs

Synthesis of aluminum nitrate (Al $(NO_3)_3\_9H_2O$), methanol (CH_3OH), and sodium hydroxide (NaOH) was done in a magnetic stirrer (make: REMI 2 MLH) and centrifuge setup (Made: REMI R-303) with a maximum speed of 3800 rpm. Phase identification of the formed particles was performed using X-ray diffraction (XRD) analysis (make: Bruker, Model No.: D2 Phaser 2nd Gen). The microstructural analysis of the developed sample was performed with the scanning electron microscope (SEM) (make: FEG quanta 250). The Zetasizer ZS90 (Malvern Instruments Ltd.) was applied for the measurement of hydrodynamic particle size of the developed nanoparticles. The Zetasizer works on the principle of dynamic light scattering to measure the particles suspended under different suspension medium. Here, distilled water (DI water) was used for the dissolution medium for the alumina nanoparticles. The mechanical-type ball milling was employed for the removal of particle agglomeration after the synthesis process. The milling was performed for 2 h with ball-to-powder ratio 2:1 with a speed of 100 rpm at normal atmospheric medium in room temperature.

In the beginning, the aluminum nitrate (Al $(NO_3)_3\_9H_2O$) of purity (assay > 99%) 25 grams and methanol (CH_3OH) were mixed properly with magnetic stirrer to get a transparent solution. The premixed sodium hydroxide (NaOH) solution is then mixed slowly to obtain a pH in the range of 10–11. The pH of 10–11 indicates the formation of aluminum hydroxide mixture. For the proper distribution of sodium hydroxide and premixed solution is stirrer for 1 h. While stirring the solution, the aluminum hydroxide particles settled down at the bottom of the jar. The obtained mixture is then centrifuged for 30 to 40 min to get white colloidal suspension of alumina solution. Before the calcination process, the obtained colloidal suspension is heated in the furnace at a temperature of 250 °C for 1 h for

Table 1 Synthesis route adopted by various authors and particle size of the Al_2O_3 NPs

Authors and year	Processing route	Synthesis temperature (°C)	Particle size (nm)
Chandradass and Bae [9]	Reverse Micelle and solgel processing route	1200	81–96
Mirjalili et al. [10]	Solgel synthesis	1200	20–30
Rogojan et al. [7]	Solgel synthesis	Above 1000	20–25
Rajaeiyan et al. [2]	Solgel and co-precipitation method	–	10–20 and 10–50
Wang et al. [8]	Homogeneous precipitation	600	27
Sadabadi et al. [11]	Combustion synthesis	450	50
Prabhakar and Samadder [12]	Combustion method	–	9–75

the drying purpose and the final calcinations are done at a temperature of 400 and 600 °C with a heating rate of 5 °C per minute for 2 h and then being cooled slowly up to room temperature. The schematic representation of the generation of the alumina nanoparticles is shown in Fig. 1.

Results and Discussion

XRD Analysis

The XRD pattern of the prepared sample is shown in Fig. 2. All the visible peaks can be indexed as Al_2O_3 (hexagonal close packing (hcp), rhombohedral structure) and can be related to the standard reference data (JCPDS: 46:1212). It was clearly observed that with the increase in calcination temperature the crystallite size of the sample increases, indicating the enhanced crystallinity. The distance between the adjacent planes can be calculated using the Bragg's equation ($n\lambda = 2d\sin\theta$), where n is the order of the diffraction, λ is the wavelength, d is the distance between the planes, and θ is the diffraction angle.

Crystallite Size Analysis

The crystallite size and microstrain value of any powder sample can be obtained through the XRD profile. The variation in the lattice strain of the sample can be depicted by the broadening of peak and intensity of the sample. The corrected instrumental broadening β_{hkl} can be calculated

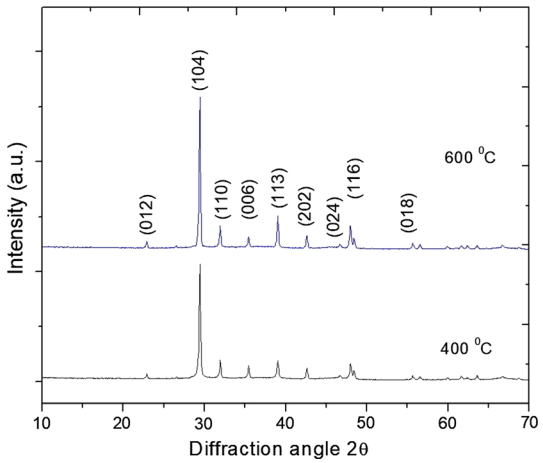

Fig. 2 XRD pattern of Al_2O_3 synthesized at temperature 400 and 600 °C

corresponding to each peak of the tested sample using the formula:

$$\beta_{hkl} = [(\beta^2_{hkl})\text{Measured} - (\beta^2_{hkl})\text{Instrumental}]^{1/2}. \quad (1)$$

In particular, the Al_2O_3 (104) peak is much stronger than the other peaks of Al_2O_3. This shows that the formed Al_2O_3 nanocrystal has a preferential (104) crystallographic orientation. The average crystal size of the Al_2O_3 can be calculated using the XRD peak width (104) and based on Debye–Scherrer relation [13]:

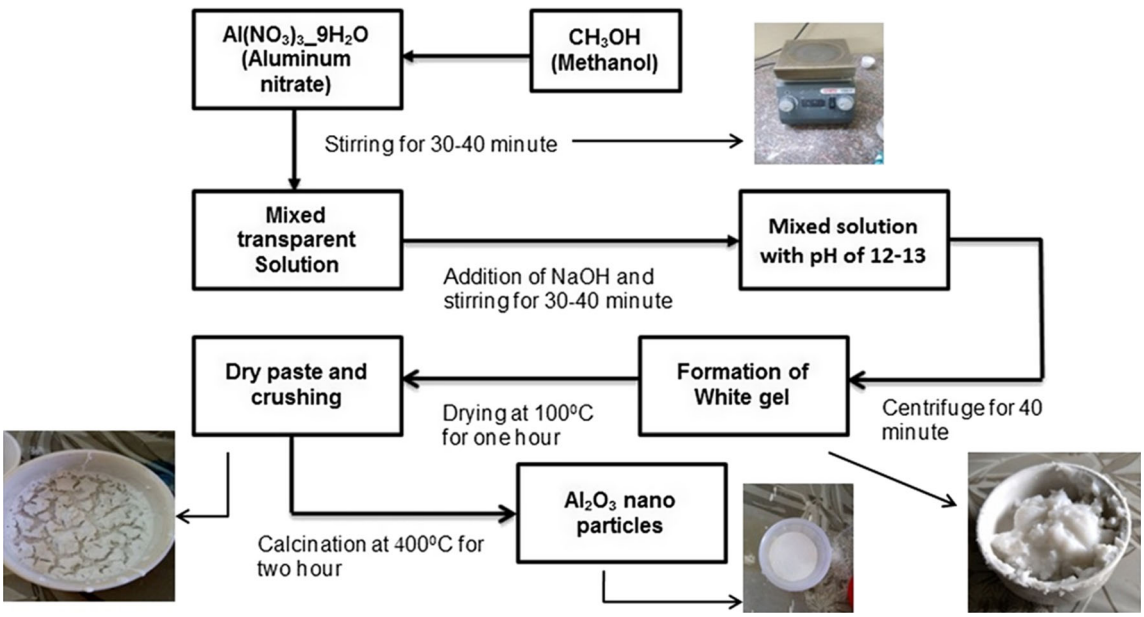

Fig. 1 Schematic for the preparation of alumina nanoparticles by the precipitation method

$$D = \frac{k\lambda}{\beta_{hkl}\cos\theta}, \tag{2}$$

where β_{hkl} is the full width half maxima corresponding to peak, K is a constant and equal to 0.90, λ is the wavelength corresponding to incident X-ray (λ = 0.1540 nm), D is the crystallite size, and θ is the Bragg's angle. The average crystallite size of the Al_2O_3 NPs calculated at 400 °C and 600 °C is equal to 53.72 nm and 72.06 nm, respectively, assuming the crystallite size to be coherent, and it is not necessary for the particle size to be the same as the crystal size. The sample dislocation density (δ) can be defined as the length of the dislocation lines per unit volume of the crystal which can be calculated as:

$$\delta = \frac{1}{D^2}, \tag{3}$$

where D is the crystallite size. The dislocation density (δ) is $3.4652 \times 10^{-4}(\text{nm})^{-2}$ at 400 °C and $1.9258 \times 10^{-4}(\text{nm})^{-2}$ at 600 °C, which clearly shows that at lower temperature the defects in the crystal per unit volume are more compared to those at higher temperature.

The crystalline growth in the annealing process can be defined by the Scott equation in assumption with homogeneous crystalline growth. During annealing, nanocrystalline growth is given by the relation: $D = C\exp(-E/RT)$, where D is the crystallite size, C is a constant, E is the activation energy for nanocrystalline growth, R is the ideal gas constant, and T is the absolute temperature. The main driving force for the interfacial reaction comes from the activation energy. Higher processing temperature leads to more activation energy, causing higher growth of the Al_2O_3 nanocrystalline.

Microstrain Analysis

Lattice strain in the crystalline structure largely affects the stability of the NPs. Figure 3 represents the variation in the strain in the XRD pattern with respect to mean line. Considering the different lattice structure of the pattern, the variation in the sample can be described [6]. The particle size, strain rate, and peak broadening are considered as independent of each other and all having Cauchy-like profile as given in the equation for crystallite size and strain rate. With the consideration of isotropy and anisotropy behavior of the crystalline material, Williamson–Hall suggested three different approaches to know the behavior of lattice strain in NPs. Williamson–Hall approach is the simple measure lattice strain and crystal size contribution. It is an approach to differentiate the size and strain induced between the peaks broadening considering the peak width as a function of 2θ. However, with the consideration of different anisotropy behavior of the crystalline material,

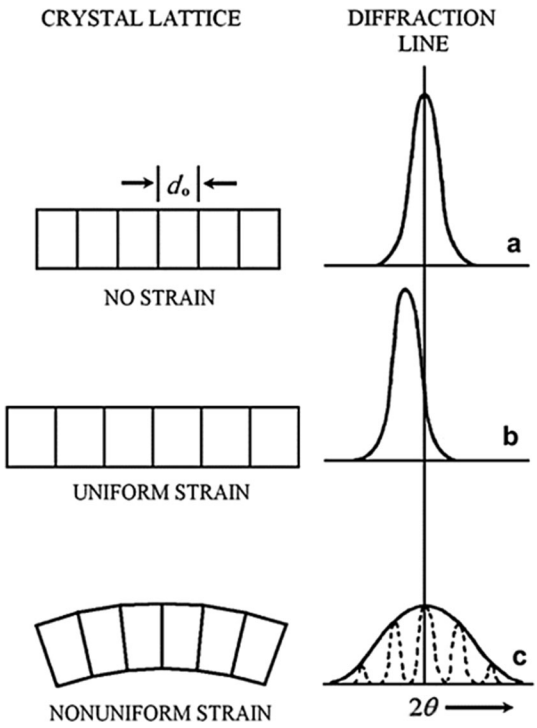

Fig. 3 Different form of XRD pattern and variation [14]

modified form of Williamson–Hall approach describes the particle behavior with uniform stress deformation model. This model utilizes the concept of Hook's law where stress is directly proportional to strain and that can be given by $\sigma = \varepsilon Y_{hkl}$ or $\varepsilon = \sigma/Y_{hkl}$ where σ is the stress of the crystal and ε is the anisotropic microstrain. All these values are dependent on the crystallographic direction and Young's modulus; Y_{hkl} is again dependent upon the directional compliance at particular temperature and directional cosine value of the crystal [14, 15]. The considerations of strain energy in the modified W–H plot largely affect the lattice strain and stress value in the NPs. The variation in the Hook's law can be modified by the use of strain energy per unit volume of the crystal. The energy density per unit volume is a function of $u = \varepsilon^2 Y_{hkl}/2$, where 'u' is the strain energy of the NPs that can be explained by the Hook's law, ε is the lattice strain, and Y_{hkl} is the Young's modulus of the crystalline structure which can be defined by the elastic compliance and directional cosine in the crystal structure [16, 17]. Figure 4 shows the variation of a single peak at diffraction angle 29.48 °C with preferential crystal orientation as (104). The strain rate for the selected peak can be calculated using the relation $\varepsilon = (\beta^*\cos\theta)/4$, where β is the full width half maxima in radian and θ is the diffraction angle. The strain calculated at 400 °C is equal to 0.5696932×10^{-3} corresponding to 600 °C

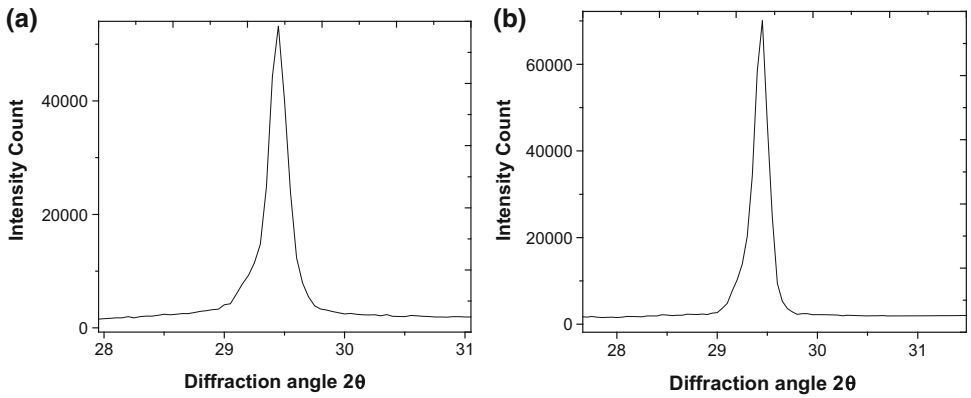

Fig. 4 Pattern of strain in XRD data **(a)** 400 °C and **(b)** 600 °C

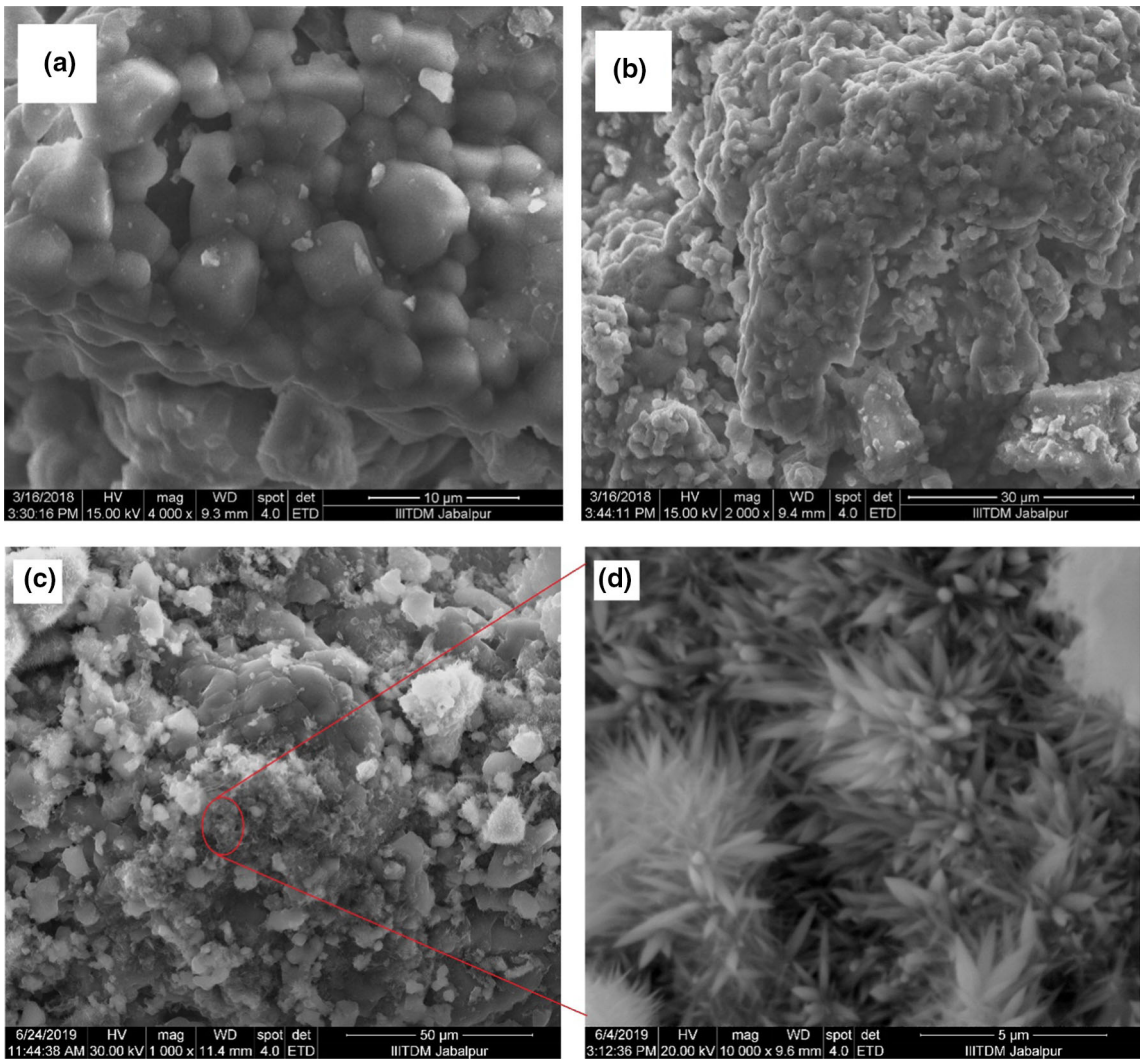

Fig. 5 SEM micrographs at different annealing temperatures before milling **a** 400 °C, **b** 600 °C and after milling **c** alumina nanoparticles at 600 °C, **d** magnified view of alumina nanoparticles at 600 °C

0.63299×10^{-3} which shows good chemical stability and low hygroscopicity.

The variation in the lattice shrinkage due to different calcination temperatures can be the reason of the strain variation in the NPs. The shrinkage of lattice can be further

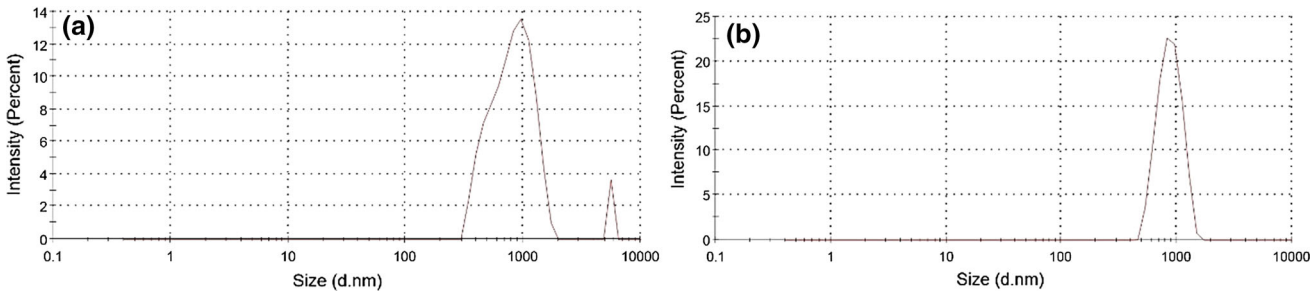

Fig. 6 Particle size analysis of the synthesized alumina nanoparticles **a** hydrodynamic particle size synthesized at 400 °C, **b** hydrodynamic particle size synthesized at 600 °C

explained with the help of the growth of nuclei and activation energy associated with the NPs. The microstrain analysis is related to the structural application of the nanoparticles. The higher microstrain value shows the strong affinity to the diffusion with the matrix material when using as reinforcement in the case of metal, ceramic, or polymer matrix composite material.

Morphology

Figure 5 shows the scanning electron micrograph (SEM) of Al_2O_3 NPs of the as-obtained powder and calcinations at different temperatures. It reveals that the Al_2O_3 NPs have a flower shape and needlelike structure. This aggregation of nanoparticles or formation of larger nanoparticles should be originated from high surface energy during the calcination process. The calcination temperature has a greater influence on the morphology of the formed nanoparticles. The crystallite size variation and particles agglomeration can be further explained by the different depending parameters during the synthesis process. The precursor temperature has greater influence on the shape formed during the synthesis process. The control on stirring speed, temperature of precursor medium during stirring, drying and calcination temperature have a strong influence on the generated nanoparticles. The use of high-energy ball mill can have a better control on the size of the powder material. To avoid particle agglomeration, mechanical ball milling, high-energy ball milling, and intensive ultrasonic and magnetic stirring are widely employed for different structural and thermal applications for the preparation of compositional alloy or nanofluid. The milled powder can be further applied for various structural and thermal applications as per the end use [18, 19]. Figure 5c and d represents the particle morphology after mechanical milling of the alumina nanoparticles. From Fig. 5c and d, it can be clearly seen that the milling process separates the particles segregation to a greater extent. The higher-magnification image shows the flower-/needlelike structure of the alumina nanoparticles. The hydrodynamic particle size was analyzed to understand the behavior of the nanoparticles under different solvent medium. Figure 6 represents the particle size analysis of the synthesized alumina nanoparticles hydrodynamic particle size synthesized at 400 ^{0}C (a), hydrodynamic particle size synthesized at 600 ^{0}C (b). The hydrodynamic particle size is generally higher than the actual particle value due to the fact of generation of small bonding between the particles when dissolving into the solvent medium [20]. However, it is considered as powerful media to understand the size of the nanoparticles for thermal application as nanofluid in microelectromechanical system (MEMS) devices. In the present case, the hydrodynamic particle size of the alumina nanoparticles synthesized at 400 and 600 °C was obtained as 839.9 nm and 882.6 nm, respectively. Also, the particle size derived from the high-magnification SEM image is obtained in the range of 24 nm.

The cost of commercially available pure form of Al_2O_3 NPs is much higher compared to that of the prepared sample. The cost associated with the synthesis of the Al_2O_3 NPs in the precipitation method is the cost of precursor medium which is much lower. For example, totally 10 grams of aluminum nitrate material leaves behind approximately 3 to 4 grams of Al_2O_3 NPs when synthesized with sodium hydroxide and methanol solvent medium. The level of purity is depending upon the processing medium (i.e., mixing medium, solution temperature, and washing medium). The selected precipitation method is cost-effective and easy to synthesize Al_2O_3 NPs compared with other processing route for the generation.

Conclusions

In this work, Al_2O_3 NPs were produced by the precipitation method, which is well repeatable and easily controlled. Analytical grade aluminum nitrate ($Al(NO_3)_3\_9H_2O$) and methanol (CH_3OH) have been used as the input materials in the experiment runs. The XRD analysis confirmed that

the Al_2O_3 NPs' crystallite size increased with increasing calcination temperature, i.e., 53 nm at 400 °C to 72 nm at 600 °C. In order to see the stability of the produced Al_2O_3 NPs, microstrain analysis has been performed which shows good chemical stability and low hygroscopicity. The economic analysis of the produced Al_2O_3 NPs as compared to purchased Al_2O_3 NPs from open market has indicated that the precipitation method is cost-effective.

References

1. T. Khalil, J. Bossert, A.H. Ashor, F.A. El-nour, 510 (2000)
2. A. Rajaeiyan, M.M. Bagheri-mohagheghi, Adv. Manuf. **1**, 176 (2013)
3. M. Tanu, Resonance **5**, 50 (2000)
4. R. Norouzbeigi, M. Edrissi, J. Am. Ceram. Soc. **94**, 4052 (2011)
5. W. Ao, J. Li, H. Yang, X. Zeng, X. Ma, Powder Technol. **168**, 148 (2006)
6. V.D. Mote, Y. Purushotham, B.N. Dole, J. Theor. Appl. Phys. **6**, 6 (2012)
7. R. Rogojan, E. Andronescu, B.S.V. Cristina Ghitulica, U.P.B. Sci. Bull. Ser. B **73**, 67 (2011)
8. M. Wang, W. Dan, J. Li, J. Ding, G. Zhou, Q. Wang, Appl. Mech. Mater. **403**, 800 (2013)
9. J. Chandradass, D. Bae, Mater. Manuf. Process. **23**, 494 (2008)
10. F. Mirjalili, M. Hasmaliza, L.C. Abdullah, Ceram. Int. **36**, 1253 (2010)
11. H. Sadabadi, A. Aftabtalab, S. Zafarian, S. Shaker, M. Ahmadipour, K. Venkateswara, Int. J. Sci. Eng. Res. **4**, 1593 (2013)
12. R. Prabhakar and S. R. Samadder, **250**, 192 (2018)
13. C.G.N.M. Suryanarayana, *X-ray Diffraction a Practical Approach* (Springer, Berlin, 1998)
14. A.K. Zak, W.H.A. Majid, M.E. Abrishami, R. Youse, Solid State Sci. **13**, 251 (2011)
15. Y.T. Prabhu, K.V. Rao, World J. Nano Sci. Eng. **4**, 21 (2014)
16. J.F. Nye, *Physical Properties of Crystals* (Oxford University Press, Oxford, 1957)
17. W.E. Tefft, J. Res. Notional Bur. Stand. A. Phys. Chem. **70**, 277 (1966)
18. N. K. Bhoi, H. Singh, S. Pratap, and P. K. Jain, in Sustain. Eng. Prod. Manuf. Technol., ed. By K. Kumar, D. Zindani, P. Davim, 1st ed. (Elsevier, 2019), pp. 3–23
19. H. Singh, P.K. Jain, N. Bhoi, S. Pratap, 3rd Int. Conf. Compos. Mater. Mater. Eng. **928**, 150 (2018)
20. E.V. Timofeeva, A.N. Gavrilov, J.M. McCloskey, Y.V. Tolmachev, S. Sprunt, L.M. Lopatina, J.V. Selinger, Phys. Rev. E Stat. Nonlinear Soft. Matter Phys. **76**, 28 (2007)